

## Supporting Text

**Theoretical Foundations.** Here, we describe the general theoretical framework that underlies our methodology; proofs and details can be found in refs. 1 and 2.

Our results apply to systems of ordinary differential equations of the following general form:

$$\begin{aligned}\dot{x}_1 &= f_1(x_1, \dots, x_n, \omega) \\ \dot{x}_2 &= f_2(x_1, \dots, x_n, \omega) \\ &\vdots \\ \dot{x}_n &= f_n(x_1, \dots, x_n, \omega),\end{aligned}$$

which describe the evolution of a set of variables  $x_1(t), \dots, x_n(t)$ ;  $\omega$  represents an external “input” signal that may be applied to the system. (In this article,  $\omega$  is always a scalar quantity, but extensions of our results to vector quantities are possible; see refs. 1 and 2.) In addition, we suppose that an “output” variable  $\eta$ , which is a function  $\eta = h(x)$  of the vector of state variables  $x = (x_1, \dots, x_n)$ , is also specified. Typically,  $\eta$  will simply be one of the variables, for instance  $\eta = x_n$ .

The role of  $\eta$  is to indicate which state variable, or combination of state variables, will be used to communicate to other systems in an interconnection or to be fed back. (It is possible to extend the results to vector outputs as well.)

It is assumed that the state  $x$  evolves in a subset  $X$  of a Euclidean space  $\mathbb{R}^n$ , called the “state-space” of the system. (Technically, one requires that the subset  $X$  be contained in the closure of its interior, see refs. 1 and 2; this is a condition that is always satisfied in biochemical applications, and allows one to impose constraints such as positivity or non-negativity.) The functions  $f_i$  and  $h$  are supposed to be differentiable in all of their arguments.

The incidence graph of a system is obtained as follows. It has  $n + 2$  nodes, labeled  $\omega$ ,  $\eta$ , and  $x_i$ ,  $i = 1, \dots, n$ . A labeled edge (an arrow with a + or – sign attached to it) is drawn whenever a variable  $x_i$  (or input  $\omega$ ) affects directly the rate of change of a variable  $x_j$ ,  $j \neq i$  (or the value of the output  $\eta$ ), and a sign is attached to each label: a + sign whenever the effect is positive and – if the effect is negative. (By definition, we do not draw edges from any  $x_i$  to itself.) That is to say, if  $f_i(x, \omega)$  is strictly increasing with respect to  $x_j$  for all  $(x, \omega)$ , then we draw a positive edge directed from vertex  $x_j$  to  $x_i$ ; if instead  $f_i(x, \omega)$  is strictly decreasing as a function of  $x_j$  for all  $(x, \omega)$ , then we draw a negative edge directed from vertex  $x_j$  to  $x_i$ ; and if  $f_i$  is independent of  $x_j$ , no edge from  $x_j$  to  $x_i$  is drawn. Similarly for edges from the vertex  $\omega$  to any vertex  $x_j$ , and from any  $x_j$  to  $\eta$ . [If an effect is ambiguous, because it depends on the actual values of the input or state variables, such as in the example  $\dot{x}_1 = (1 - x_1)x_2 + \omega$ , where  $f_1(x_1, x_2, \omega) = (1 - x_1)x_2 + \omega$  is an increasing function of  $x_2$  if  $x_1 < 1$ , but is a decreasing function of  $x_2$  if  $x_1 > 1$ , then a graph cannot be drawn and our method as described here does not apply.] We define the sign of a path (the individual edges transversed in any direction, forward or backwards) as the product of the signs along it, and say simply that the corresponding path is positive or negative.

For example, the following system:

$$\begin{aligned}\dot{x}_1 &= -x_1 + \frac{1}{1+\omega} \\ \dot{x}_2 &= -x_1 - x_2 + x_3 - \omega \\ \dot{x}_3 &= -x_1 + x_2 - x_3\end{aligned}$$

with output  $\eta = x_3 - x_1$  has the incidence graph shown in Fig. 6a (ignore, for now, the

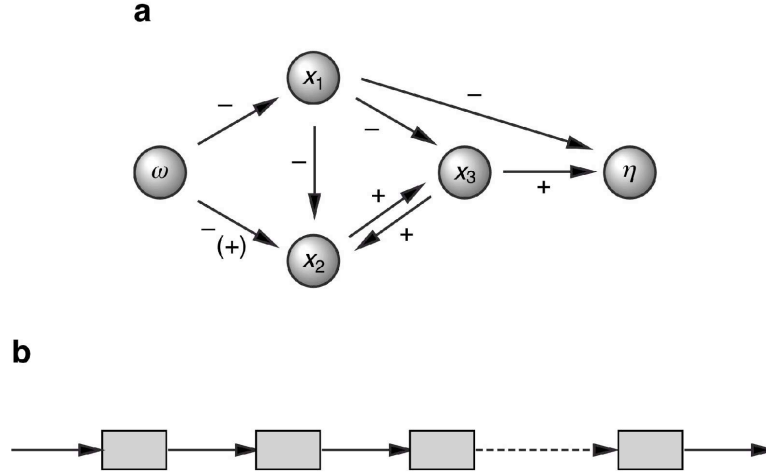


Fig. 6. (a) Example of an incidence graph. (b) A cascade of subsystems.

positive sign in parenthesis). Note, for instance, that the sign of the path  $x_1, x_3, x_2$  is negative (one negative and one positive edge), and the sign of the path (a loop, since the beginning and endpoint coincide)  $\omega, x_1, x_2, \omega$  is also negative (product of three negative signs).

We define a system to be “strongly I/O monotone” provided that conditions i-iv, as described earlier, hold for the incidence graph of the system. (It is not necessary for the strict decrease or increase conditions to hold at boundary points, where some concentrations may be zero, as long as every solution of the closed loop system is guaranteed to enter the interior. Also, a far weaker condition, expressed mathematically in terms of convex cones, is sufficient, see ref. 1.) For example, a system whose graph is as shown in Fig. 6a is not monotone, because the the loop  $\omega, x_1, x_2, \omega$  is negative (or because there is a path from  $\omega$  to  $\eta$ , namely  $\omega, x_2, x_3, \eta$ , that is negative). On the other hand, if the second equation had been  $\dot{x}_2 = -x_1 - x_2 + x_3 + \omega$  instead of  $\dot{x}_2 = -x_1 - x_2 + x_3 - \omega$ , then the graph would have a positive sign on the  $\omega$  to  $x_2$  edge (+ in parentheses), and the system would have been monotone.

Finally, we say that a system has a monostable steady-state response to constant inputs, or that it has a well-defined steady-state I/O characteristic, provided that, for each possible constant input  $\omega$ , there exists a (unique) globally asymptotically stable equilibrium, denoted  $k_x(\omega)$ , and the nondegeneracy condition  $\det Df(k_x(\omega), \omega) \neq 0$  [ $Df$  indicates the Jacobian with respect to  $x$ ] holds at the corresponding equilibrium. The

I/O characteristic is, by definition, the output corresponding to this steady state, that is  $k_\eta(\omega) = h(k_x(\omega))$ . The main theorem in ref. 1 is as follows. (The theorem in that reference is more general, but this special case is sufficient for our purposes.) Suppose that the system:

$$\dot{x} = f(x, \omega), \quad \eta = h(x)$$

has a well-defined I/O characteristic and is strongly I/O monotone. Consider the unitary positive-feedback interconnection  $\omega = \eta$ :

$$\dot{x} = f(x, h(x)).$$

Then, the steady states of this closed loop system are in a 1-1 correspondence with the fixed points of the I/O characteristic. Moreover, if the derivative  $k'(\omega) \neq 1$  at any fixed point  $\omega$ , and if all trajectories of the system are bounded, then for all initial conditions, except at most those belonging to a set of measure zero, solutions converge to the set of equilibria of  $\dot{x}$  corresponding to inputs for which  $k'(\omega) < 1$ . (Boundedness of trajectories is often automatic in biochemical models, because of conservation of mass and other constraints.)

A very useful fact that helps in verifying our conditions *A* and *B* is that monotonicity and existence of characteristics are always true for cascades of systems (under some mild technical mathematical conditions, see ref. 2, provided only that every individual subsystems in the cascade satisfies the requirements. Cascades are systems composed of subsystems, the output of each of which is an input to the next subsystem (Fig. 6*b*).

**Monotonicity in the MAPK Cascade Model.** We can generalize the results shown in Fig. 5*b* to any system with the generic form:

$$\left. \begin{aligned} \dot{x}_1 &= -\omega\theta_1(x_1) + \theta_2(M - x_1 - x_2) \\ \dot{x}_2 &= \omega\theta_3(M - x_1 - x_2) - \theta_4(x_2) \end{aligned} \right\} := f(x_1, x_2, \omega),$$

where the  $\theta$ s denote arbitrary differentiable functions satisfying  $\theta'(r) > 0$  and  $\theta_i(0) = 0$  [which is true for our example where  $\theta_i(r) = \frac{V_i r}{K_i + r}$ , and where we take “ $x_1$ ” to be  $y_1$  or  $z_1$ , and “ $x_2$ ” to be  $y_3$  or  $z_3$ ] and evolving on a state space given by the following triangle:

$$X = \Delta := \{[x_1, x_2] : x_1 \geq 0, x_2 \geq 0, x_1 + x_2 \leq M\}.$$

The graph associated with the system is given by that shown in Fig. 5*b*. Inspection of this graph proves monotonicity. See ref. 1 for generalizations to an even wider class of systems.

**Parameterizing the MAPK Cascade Model.** Here, we present the experimental rationale for the MAPK cascade model shown in Fig. 5, and for the particular parameters we have chosen for the model.

The basic premise of the model is that all of the enzymatic reactions reach a kinetic steady state rapidly, and therefore can be approximated by Michaelis-Menten expressions for reaction rate as a function of protein substrate concentration. A similar model (except with negative feedback rather than positive feedback) has been presented by Kholodenko (3).

The activation of p42 MAPK by MEK is assumed to occur via a nonprocessive, dual phosphorylation mechanism, based on *in vitro* studies (4-5). There is not an obligatory order for the phosphorylations, but *in vitro* the tyrosine phosphorylation generally precedes the threonine phosphorylation (4), so we suppose there are three main MAPK species—unphosphorylated MAPK ( $z_1$ ), MAPK-YP ( $z_2$ ), and MAPK-YP/TP ( $z_3$ ), with the fourth potential species (MAPK-TP) ignored. The activities of monophosphorylated and unphosphorylated MAPK [ $\sim 2\%$  and  $\sim 0.002\%$  that of the  $z_3$  form, respectively (6)] are ignored as well. The dephosphorylations are assumed to occur in separate steps, as indicated from experiments in *Xenopus* oocytes and extracts (7).

The mechanism of MEK activation is somewhat less well understood. The phosphorylation of MEK by Mos appears to be nonprocessive *in vitro* (8), and mutational studies suggest that MEK must be dual-phosphorylated to become fully active. However, other studies indicate that monophosphorylated MEK may possess substantial activity (9). Here we have assumed that only MEK-PP ( $y_3$ ) is active.

The activation of Mos is poorly understood. It is likely to involve changes in mRNA translation (10-11), in protein stability (12), and possibly other types of regulation as well. In the absence of more detailed information on the mechanism of Mos activation, we have assumed a simplified mechanism, where Mos synthesis is directly stimulated by active MAPK ( $z_3$ ).

This results in the following equations:

$$\begin{aligned}
\dot{x} &= -\frac{V_2 x}{K_2 + x} + vV_0 z_3 x + V_1 \\
\dot{y}_1 &= \frac{V_6 y_2}{K_6 + y_2} - \frac{V_3 x y_1}{K_3 + y_1} \\
\dot{y}_2 &= \frac{V_3 x y_1}{K_3 + y_1} + \frac{V_5 y_3}{K_5 + y_3} - \frac{V_4 x y_2}{K_4 + y_2} - \frac{V_6 y_2}{K_6 + y_2} \\
\dot{y}_3 &= \frac{V_4 x y_2}{K_4 + y_2} - \frac{V_5 y_3}{K_5 + y_3} \\
\dot{z}_1 &= \frac{V_{10} z_2}{K_{10} + z_2} - \frac{V_7 y_3 z_1}{K_7 + z_1} \\
\dot{z}_2 &= \frac{V_7 y_3 z_1}{K_7 + z_1} + \frac{V_9 z_3}{K_9 + z_3} - \frac{V_8 y_3 z_2}{K_8 + z_2} - \frac{V_{10} z_2}{K_{10} + z_2} \\
\dot{z}_3 &= \frac{V_8 y_3 z_2}{K_8 + z_2} - \frac{V_9 z_3}{K_9 + z_3}.
\end{aligned}$$

The assumed values for the protein concentrations, rate constants, and Michaelis constants are shown in Table 1. These parameters were chosen to be consistent with experimentally determined abundance and kinetic data, where such data are available (13); to reproduce the activation and inactivation kinetics seen in *Xenopus* oocyte extracts treated with recombinant myelin basic protein-Mos (MBP-Mos) (to turn the cascade kinases on) or EDTA (to turn the cascade kinases off) (unpublished data); and, most importantly, to reproduce the experimentally determined data on the steady-state activity of p42 MAPK ( $z_3$ ) as a function of the concentration of MBP-Mos in extracts (14). The

importance of this last criterion comes from the fact that our theorem shows that the shape of the characteristic for the open-loop system (Fig. 5c), which is similar to that of the measured p42 MAPK stimulus/response curve (Fig. 5d), determines the stability behavior of the closed loop system. Indeed, the model reproduces the experimental data well (Fig. 5d).

It is important to note that if nonphosphorylated MAPK ( $z_1$ ) can act as a competitive inhibitor of the phosphorylation of monophosphorylated MAPK ( $z_2$ ) by active MEK ( $y_3$ ), and MEK is operating close to saturation, then the system will not necessarily be monotone. The same is true if bisphosphorylated MAPK ( $z_3$ ) can act as a competitive inhibitor of monophosphorylated MAPK ( $z_2$ ) for access to the relevant MAPK phosphatase, assuming the phosphatase is operating close to saturation.

**Other Feedback Loops and Relation to Phase-Plane Analysis.** For simplicity of exposition, we have described our results for feedback systems in which the output is fed back, with no further modifications, as an input (except perhaps for a multiplicative factor  $v$ ). More complicated feedback loops may be studied with the same techniques, however, by a reduction to unity feedback.

Suppose that we are given a feedback loop as shown in Fig. 7a, Left, composed of two systems whose I/O characteristics are denoted  $f$  and  $g$ . System  $g$  responds to input  $\omega$ , producing output  $z$ , which is fed into the system  $f$ , which in turn produces an output  $\eta$ , and this is used as an input  $\omega = \eta$  to the first system. We may alternatively view this system as the system obtained by closing the loop ( $\omega = \eta$ ) on the composite open-loop system formed by the cascade of the two original subsystems, see Fig. 7a, Right. Observe that the I/O characteristic  $k(\omega)$  of the cascade is the composition  $k = f \circ g$  of the two individual characteristics, that is,  $k(\omega) = f(g(\omega))$ . Steady states of the closed loop correspond to pairs  $\omega, z$  such that  $f(z) = \omega$  and  $g(\omega) = z$ , or equivalently to values  $\omega$  of the input such that  $f^{-1}(\omega) = g(\omega)$ . We may find these steady states, therefore, by intersecting the graphs of  $f^{-1}$  and  $g$  (Fig. 7b). Stable points of the closed loop system correspond to points where the slope of  $g$  is less than the slope of  $f^{-1}$ , because the condition  $k'(\omega) < 1$  when  $k$  is the composition  $k(\omega) = f(g(\omega))$ , is equivalent to  $f'(g(\omega))g'(\omega) < 1$ , which is, in turn, equivalent to  $g'(\omega) < (f^{-1})'(\omega)$ . [Observe that this rule is consistent with the special case when  $f$  is the identity mapping, in which case  $f^{-1}(\omega) \equiv 1$  and we recover our previous condition  $g'(\omega) < 1$ .]

It is instructive to compare our conclusions with a routine phase plane analysis of the (very special, and only 2D) system:

$$\begin{aligned}\dot{z} &= -z + g(\eta) \\ \dot{\eta} &= -\eta + f(z),\end{aligned}$$

which can be seen as the feedback interconnection of a monotone system with I/O characteristic  $g$  and a monotone system with I/O characteristic  $f$ . At any steady state  $(z_0, \eta_0)$  we have that  $f(z_0) = \eta_0$  and  $g(\eta_0) = z_0$ . The Jacobian at such a point is:

$$\begin{pmatrix} -1 & g'(\eta_0) \\ f'(z_0) & -1 \end{pmatrix}$$

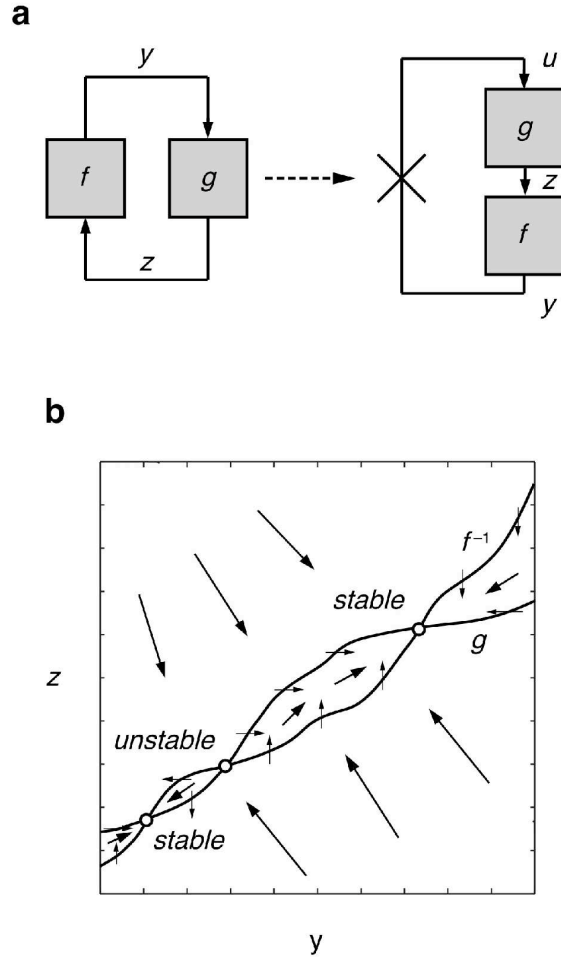


Fig. 7. (a) Feedback interconnection as unity feedback. (b) Characteristics of  $g$  and  $f^{-1}$  are nullclines for a 2D system

which has negative trace and determinant  $1 - g'(\eta_0)f'(z_0) = 1 - g'(\eta_0)f'(g(\eta_0))$ . This determinant is positive, insuring (local) stability, if and only if  $g'(\eta_0)f'(g(\eta_0)) < 1$ , which amounts to our condition  $g'(\omega) < (f^{-1})'(\omega)$  at  $\omega = \eta_0$ .

In fact, global stability can be analyzed in this case as well. We may draw nullclines and sketch vector field directions very easily (Fig. 7b). It is then clear from this sketch that there is global stability to the states at which the condition  $g'(\omega) < (f^{-1})'(\omega)$ . Our results hold for systems in arbitrary dimensions, and not just in this special form, provided that monotonicity and existence of I/O characteristics have been verified.

**Further Remarks: Robustness and Other Feedback Structures.** Our method is fairly robust to biochemically plausible variations in the models being considered. It can be mathematically shown that the form of the characteristic is preserved under small perturbations in the parameters of a model. Moreover, in the MAPK example, we used a standard model based on quasi-steady state assumptions; if these fast intermediate reactions are kept in the model, one may still apply our methodology.

Complex signaling and regulatory networks involve multiple and interlocked positive and feedback loops. Much further research will be needed to obtain a complete set of tools to analyze such complex systems in their full generality. Our approach is based on the idea of breaking up loops and reconstituting the system by analyzing the various interconnections. In particular, negative feedback interconnections, which may give rise to oscillations, are studied in detail in ref. 2.

**Table 1. Kinetic parameters used in the MAPK cascade model**

Parameter		Value	Source
$y_{tot}$	total MEK concentration	1,200 nM	Experimentally determined (13)
$z_{tot}$	total p42 MAPK concentration	300 nM	Experimentally determined (13)
$V_0$	$\dots \xrightarrow{\text{MAPK-PP}} \text{Mos}$	$0.0015 \text{ sec}^{-1} \cdot \text{nM}^{-1}$	Arbitrary
$V_1$	$\dots \rightarrow \text{Mos}$	$0.000002 \text{ sec}^{-1}$	Arbitrary
$V_2$	$\text{Mos} \rightarrow \dots$	$1.2 \text{ nm} \cdot \text{sec}^{-1}$	Arbitrary
$K_2$	$\text{Mos} \rightarrow \dots$	200 nM	Arbitrary
$V_3$	$\text{MEK} \xrightarrow{\text{Mos-P}} \text{MEK-P}$	$0.064 \text{ sec}^{-1}$	Consistent with kinetics of MEK activation in Mos-treated extracts (unpublished data)
$K_3$	$\text{MEK} \xrightarrow{\text{Mos-P}} \text{MEK-P}$	1,200 nM	Arbitrary; equal to the measured total abundance of MEK (13)
$V_4$	$\text{MEK-P} \xrightarrow{\text{Mos-P}} \text{MEK-PP}$	$0.064 \text{ sec}^{-1}$	Consistent with kinetics of MEK activation in Mos-treated extracts (unpublished data)
$K_4$	$\text{MEK-P} \xrightarrow{\text{Mos-P}} \text{MEK-PP}$	1,200 nM	As for $K_3$ .
$V_5$	$\text{MEK-PP} \rightarrow \text{MEK-P}$	$5 \text{ nm} \cdot \text{sec}^{-1}$	Consistent with kinetics of MEK inactivation in EDTA-treated extracts (unpublished data)
$K_5$	$\text{MEK-PP} \rightarrow \text{MEK-P}$	1,200 nM	As for $K_3$ .
$V_6$	$\text{MEK-P} \rightarrow \text{MEK}$	$5 \text{ nm} \cdot \text{sec}^{-1}$	As for $V_5$ .
$K_6$	$\text{MEK-P} \rightarrow \text{MEK}$	1,200 nM	As for $K_3$ .
$V_7$	$\text{MAPK} \xrightarrow{\text{MEK-PP}} \text{MAPK-P}$	$0.06 \text{ sec}^{-1}$	Experimental estimates with activated recombinant MEK are $\sim 0.024 \text{ sec}^{-1}$ (ref. 15)
$K_7$	$\text{MAPK} \xrightarrow{\text{MEK-PP}} \text{MAPK-P}$	300 nM	Experimental estimates with activated recombinant MEK are $\sim 330 \text{ nM}$ (15)
$V_8$	$\text{MAPK-P} \xrightarrow{\text{MEK-PP}} \text{MAPK-PP}$	$0.06 \text{ sec}^{-1}$	As for $V_7$ .
$K_8$	$\text{MAPK-P} \xrightarrow{\text{MEK-PP}} \text{MAPK-PP}$	300 nM	Experimental estimates with activated recombinant MEK are $\sim 330 \text{ nM}$ (15)
$V_9$	$\text{MAPK-PP} \rightarrow \text{MAPK-P}$	$5 \text{ nm} \cdot \text{sec}^{-1}$	Together with the assumed value of $K_9$ (300 nM), this implies a half-time of $\sim 50 \text{ sec}$ for this dephosphorylation reaction. Experiments indicate an apparent half-time on the order of 5 min (7).
$K_9$	$\text{MAPK-PP} \rightarrow \text{MAPK-P}$	300 nM	Based on unpublished evidence.
$V_{10}$	$\text{MAPK-P} \rightarrow \text{MAPK}$	$5 \text{ nm} \cdot \text{sec}^{-1}$	As for $V_9$ .
$K_{10}$	$\text{MAPK-P} \rightarrow \text{MAPK}$	300 nM	As for $K_9$ .

1. Angeli, D. & Sontag, E.D. (2003) *Syst. and Control Lett.*, in press.
2. Angeli, D. & Sontag, E.D. (2003) *IEEE Trans. Autom. Control* **48**, 1684–1698.
3. Kholodenko, B.N. (2000) *Eur. J. Biochem.* **267**, 1583-1588.
4. (1997) Ferrell, J.E., Jr. & Bhatt, R.R. *J. Biol. Chem.* **272**, 19008-19016.
5. Burack, W.R. & Sturgill, T.W. (1997) *Biochemistry* **36**, 5929-5933.
6. Lew, J. (2003) *Biochemistry* **42**, 849-856.
7. Sohaskey, M.L. & Ferrell, J.E., Jr. (1999) *Mol. Biol. Cell* **10**, 3729-3743.
8. Resing, K.A., Mansour, S.J., Hermann, A.S., Johnson, R.S., Candia, J.M., Fukasawa, K., Vande Woude, G.F. & Ahn, N.G. (1995) *Biochemistry* **34**, 2610-2620.
9. Alessi, D.R., Saito, Y., Campbell, D.G., Cohen, P., Sithanandam, G., Rapp, U., Ashworth, A., Marshall, C.J. & Cowley, S. (1994) *EMBO J.* **13**, 1610-1619.
10. Barkoff, A., Ballantyne, S. & Wickens, M. (1998) *EMBO J.* **17**, 3168-3175.
11. Howard, E.L., Charlesworth, A., Welk, J. & MacNicol, A.M. (1999) *Mol. Cell. Biol.* **19**, 1990-1999.
12. Castro, A., Peter, M., Magnaghi-Jaulin, L., Vigneron, S., Galas, S., Lorca, T. & Labbe, J.C. (2001) *Mol. Biol. Cell* **12**, 2660-2671.
13. Ferrell, J.E., Jr. (1996) *Trends Biochem. Sci.* **21**, 460-466.
14. Huang, C.-Y.F. & Ferrell, J.E., Jr. (1996) *Proc. Natl. Acad. Sci. USA* **93**, 10078-10083.
15. Mansour, S.J., Candia, J.M., Matsuura, J.E., Manning, M.C. & Ahn, N.G. (1996) *Biochemistry* **35**, 15529-15536.